Adventures in boron chemistry – the prediction of novel ultra-flexible boron oxide frameworks

Neil L. Allan and Harvey J. A. Dale

School of Chemistry, University of Bristol, Cantock's Close, Bristol, BS8 1TS, UK

Judy N. Hart

School of Materials Science and Engineering, UNSW Sydney, NSW 2052, Australia

Frederik Claeyssens

Materials Science and Engineering Department, Kroto Research Institute, University of Sheffield, Broad Lane, Sheffield, S3 7HQ, UK

Abstract

Recent periodic density functional calculations have predicted the existence of ultra-flexible low-energy forms of boron oxides in which rigid boron-oxygen heterocycles are linked by flexible B-O-B bridges. The minima in the energy landscapes of these frameworks are remarkably broad, with widths in excess of those of many hybrid metal-organic frameworks. Enormous changes in cell volume, which can exceed a factor of two, are accompanied by negligible changes in energy. Here we explore the underlying reasons for this behaviour using molecular electronic-structure calculations, periodic density functional theory and template-based geometric simulations.

The angular flexibility of the B-O-B bridge depends only upon the geometry of the local B_2O_5 unit independent of the configuration of neighbouring bridges. Unique cooperativity between bending and twisting motions of the bridges leads to considerable anisotropy in framework flexibility. Exceptional flexibility is conferred not only by the intrinsic bending flexibility of the bridges but by topological factors, crucially the relaxation of torsional constraints when B_3O_3 rings are present. We test these conclusions by showing how the flexibility of the frameworks can be tuned by decoration with isoelectronic rings.

The new nanoporous boron oxides presented in this work are predicted to be potential novel guest-host materials because of their flat energy landscapes. Furthermore, such structures can be generated systematically from silicates by substitution of $B_2O_5^{4-}$ for SiO_4^{4-}. A borate analogue of β-cristobalite is shown to be isoenergetic with the known B_2O_3-I polymorph. We raise the possibility of new families of frameworks and zeolite analogues.

Introduction

Standard textbooks assert that a solid is distinguished from other states of matter by a fixed volume, a key principle introduced early on in any general science course. This reflects the typical form of the energy landscapes of solid-state compounds which have well-defined minima at specific volumes, corresponding to different phases.

Nevertheless, recent years have seen substantial and growing attention paid to nanoporous hybrid metal-organic frameworks (MOFs)[1], which contain metal centres connected though multidentate organic ligands, forming three-dimensional networks. Numerous crystal structures are adopted by such systems and they have many potential applications as host-guest materials, including gas storage, fluid separation, drug delivery, sensors and as heterogeneous catalysts[2,34,5,6]. The organic ligands can provide framework flexibility, and flexible MOFS exhibit structures which are *topologically identical* but with *very different unit cell volumes* and consequent pore sizes[7,8,9,10]. For example, calculations[11] on the flexible MOF MIL-53(Cr) ($Cr_4(OH)_4(C_8H_4O_4)$) have revealed a structure with a small pore volume almost equienergetic with a topologically equivalent form with large pores and a unit cell volume larger by a factor of ≈1.6. Mil-88 is another example, where due to their rotational freedom, carboxylic acid groups play the role of a knee-cap.[12,13] This structural flexibility can allow guest molecules to travel through pores that would otherwise be too small and rigid to allow them to pass and also gives rise to intriguing mechanical properties such as negative thermal expansion[14,15].

This framework flexibility is generally less marked in nanoporous materials which are solely inorganic, such as zeolites. The influence of flexibility on properties such as adsorption has only been studied in a few such systems including silicate-1[16]. In this paper we examine and predict inorganic boron-oxygen frameworks which show unprecedented flexibility. The minima in the energy landscapes for these three-dimensional crystalline structures are very broad; in some cases, the frameworks can triple their volume with negligible changes in energy, with no change in connectivity and topology. Tripling of volume also takes place in MIL-88, but accompanied by adsorption of solvent[12,13]; such ranges in volume are far larger than that[11] for MIL-53Cr. We probe the underlying atomic mechanisms that permit such extraordinary behaviour, demonstrate how to tune the flexibility of the structures in a number of different ways and discuss the wider implications of our results.

Diboron trioxide (B_2O_3) has so far been observed to adopt only a select few crystalline structures and an amorphous phase.[17] The polymorph B_2O_3-I (α-B_2O_3, space group $P3_1$) is obtained at relatively low pressures, and comprises interconnected ribbons of trigonal BO_3 units.[18] The application of higher pressure (≈7 GPa) leads to an increase in the coordination number of boron from three to four and the corresponding transformation to orthorhombic B_2O_3-II (β-B_2O_3, space group *Cmc2*), a crystalline network of corner-sharing BO_4 tetrahedra.[19] The vitreous phase of diboron trioxide, B_2O_3-g (γ-B_2O_3), is a disordered covalent framework of trigonal BO_3 units and bridged boroxyl rings (B_3O_6), with the most recent experimental assessments assigning approximately 70-75% of boron atoms to boroxyl rings.[20,21].

Until recently, the rationale for such limited polymorphism in B_2O_3 was that a significant proportion of these theoretical structures – including B_2O_3-0, proposed on the basis of molecular dynamics simulations to account for the abnormal thermomechanical behaviour of vitreous B_2O_3 – were supposedly thermodynamically inaccessible (> 23.8 kJ mol^{-1} less stable than B_2O_3-I)[22,23]. However, later *ab initio* calculations by Ferlat *et al.*[17] and Claeyssens *et al.*[24] have unveiled the existence of various low-energy B_2O_3 polymorphs. Indeed, the potential existence of numerous low-energy polymorphs of B_2O_3 had been suggested by Ferlat *et al.*[17] as a rationalisation of its ease of vitrification. Attention has been drawn previously in theoretical studies[25,26,27,28] to possible nanoporous polymorphs of other oxides such as ZnO and MgO, but, in contrast to broadly similar predicted structures for boron oxides, these are all much considerably higher in internal energy than the known structures and do not show any exceptional flexibility.

Thus our starting point in this paper is the (small) set of periodic calculations on eight possible structures for B_2O_3 reported in our earlier work[24]. Figure 1 shows the previously reported energy-volume curves, calculated using periodic density functional theory. Structure A corresponds to B_2O_3-I. Structures, B, C and D were built from BO_3 units by interconnecting 2D sheets with B-O-B bridges, as discussed in ref. 24. This generated three nanoporous structures with different numbers of BO_3 units surrounding the nanopores, with the number of such units around the pores increasing from B to D. Structure B is equivalent

to that denoted T2 in ref. 17, and structures C and D were constructed from arrangements known to occur in other networks ($B_6O_9(en)_2@(H_2en)Cl_2$, $B_6O_9(en)$ and $(H_2en)_2(Hen)_2B_{16}O_{27}$)[29,30].

The other four structures (A-R, B-R, C-R and D-R) are analogous to A-D, formed by replacing all the boron atoms in each structure in turn by boroxyl (B_3O_3) rings. This is shown in Figure 2 for A (B_2O_3-I) and A-R (Figures 2a and b). We stress this interchange of three-coordinate building blocks preserves overall stoichiometry, and the number of building blocks surrounding the nanopores is also the same whether the blocks are single boron atoms or B_3O_3 rings. Construction of D-R by interconnecting 2D sheets is shown in Figures 2c and 2d.

The calculated unit cell parameters of B_2O_3-I (A) were in good agreement with experiment. All seven other structures examined are comparable in energy with B_2O_3-I; energies (per mole of atoms) at the minima in the energy-volume plots all lie within 3 kJ mol^{-1} of each other, as shown in Figure 1.

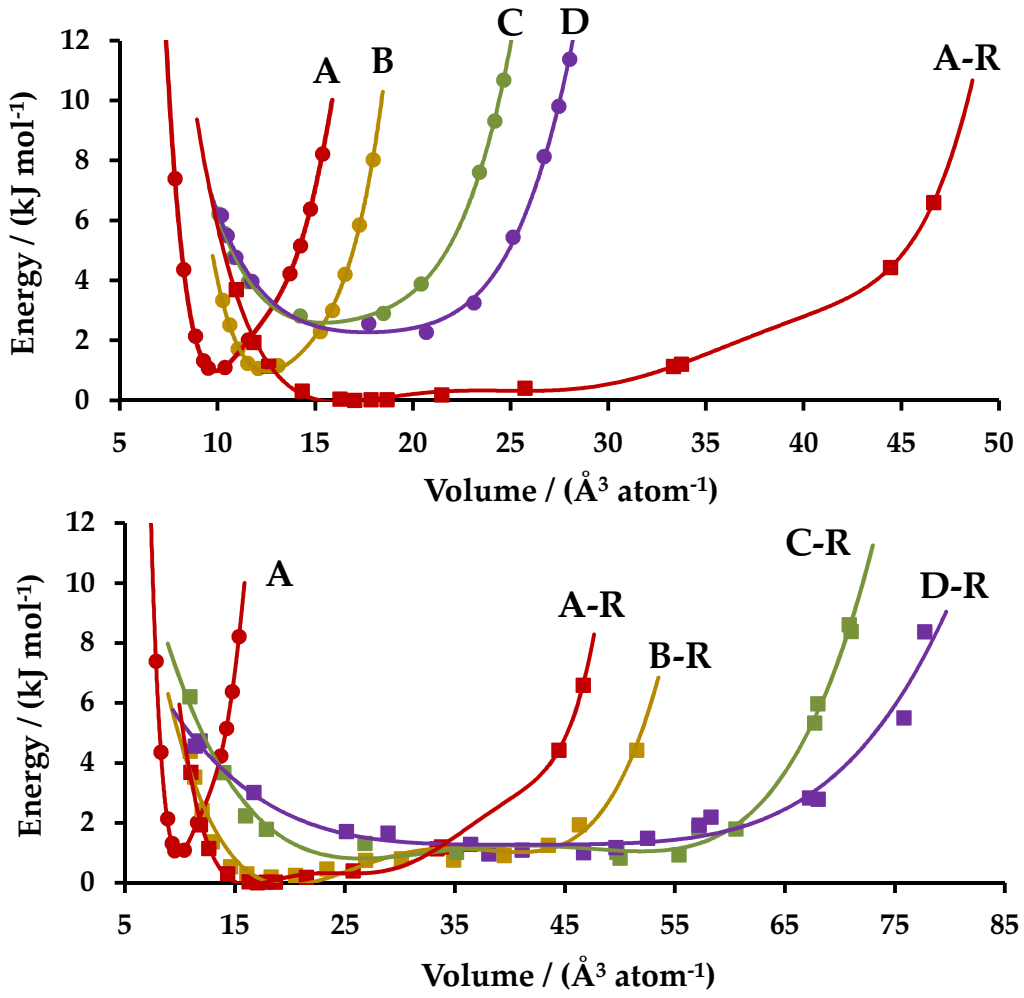

Figure 1: Energy (per mole of atoms) vs. volume curves for (a) the four B_2O_3 structures A-D and (b) their analogues with B_3O_3 rings replacing BO_3 units, A-R, B-R, C-R, D-R. Structure A is the experimentally known structure of B_2O_3-I. All energies are plotted relative to the lowest energy calculated, the minimum for Structure A-R. Structure A is included in both plots for comparison. The interconnecting lines are 4th order polynomial fits in order to guide the eye.

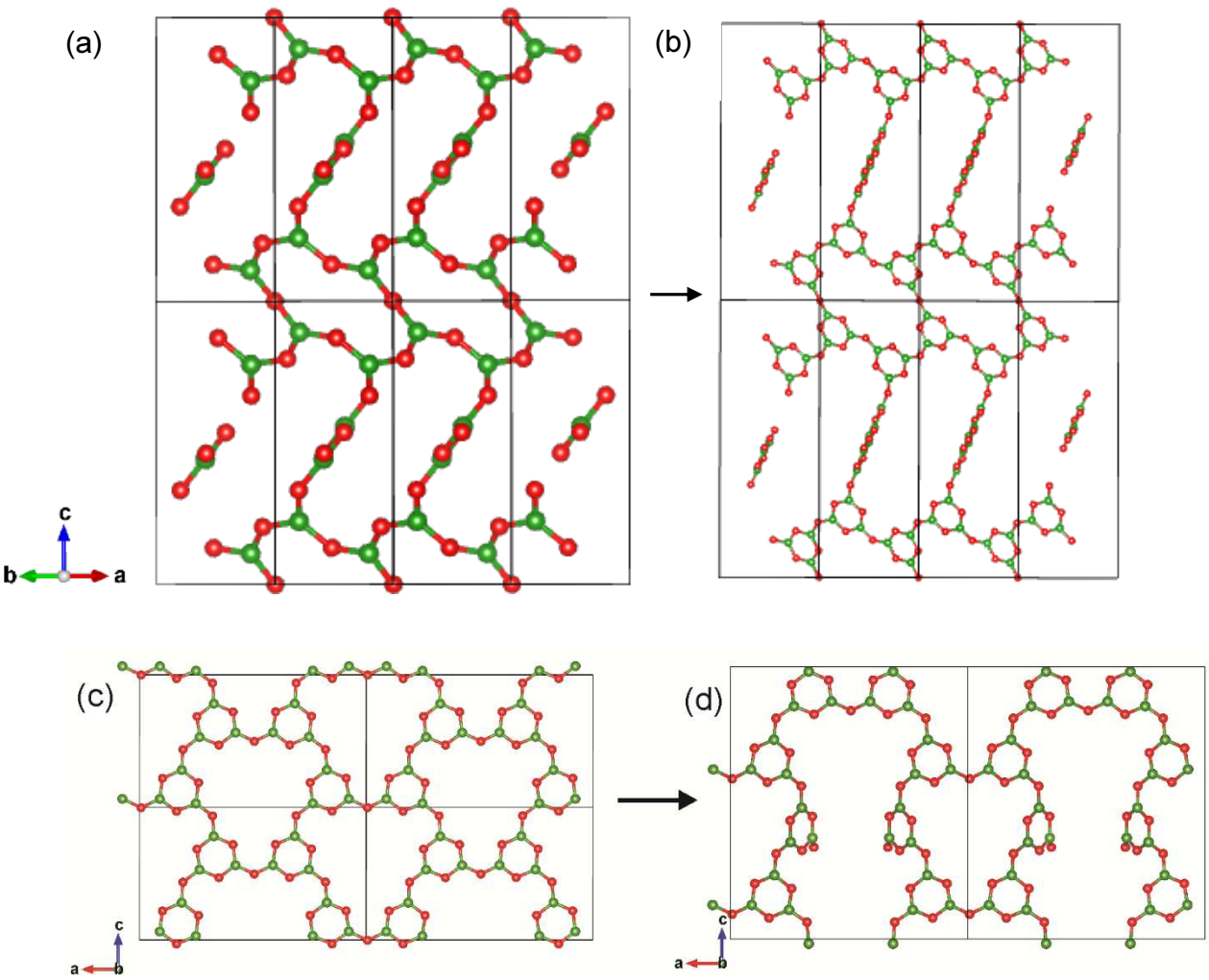

Figure 2: (a) Structure of B_2O_3-I (A in Figure 1) and (b) the analogous B_3O_3-ring based structure A-R. (c) 2D sheet used to generate (d) Structure D-R. To construct the 3D structure of D-R shown in (d) from the sheet in (c), one intralayer B-O-B bond per unit cell was replaced by one interlayer B-O-B bond. Boron atoms are green and oxygen atoms are red. Black lines show the unit cell boundaries.

All seven structures, as yet unknown in crystalline form (B-D, and R-forms), are considerably more flexible than B_2O_3-I. The energy-volume curves for all the R-forms (Figure 1b) are all remarkably flat, varying by less than 5 kJ mol^{-1} over an enormous volume range, which for D-R is as large as 12 – 75 $Å^3$ $atom^{-1}$. A predicted low energy form of boron monoxide, containing six-membered B_4O_2 rings, also exhibits very similar behaviour[31]. The existence of such flexible structures can be readily invoked to rationalise the difficulty faced by researchers in constructing a theoretical model of vitreous B_2O_3 capable of both satisfying the experimental boroxyl content and also replicating the observed density (~1.8 g cm^{-3}).[32]

We can thus predict a large number of virtually equienergetic structures with very broad energy landscapes. The underlying cause of the width of the landscapes must be associated with the electronic structure of the B-O-B bridges between the boroxyl rings. Analogous flexibility is seen in molecular forms; for example, calculations at the MP2/6-311++G(d,p) level show that all conformations of $(HO)_2B\text{-}O\text{-}B(OH)_2$ for B-O-B angles larger than 120˚ are within 30 kJ mol^{-1} of each other. Such angular flexibility is integral to the broad energy-volume landscapes observed in the solid state, but by itself is unable to account for the substantial widening of the landscapes observed for the boroxyl-decorated systems A-R to D-R.

In this paper we more fully elucidate the nature of this behaviour and study the relationship between the intrinsic flexibility of these frameworks and the underlying electronic structure of the units from which they are built. Plane-wave density functional theory calculations are complemented by molecular electronic structure calculations and template-based geometric simulations of the solid state. We subsequently use this information to predict further structures and show how the breadth of the energy landscape may be tuned.

Theoretical Methods

Periodic *ab initio* calculations were conducted on the solid-state structures with the CASTEP program, using plane-wave density functional theory, the GGA approximation and the Perdew-Wang 91 (PW91) exchange-correlation functional.[33, 34, 35] Core electrons were simulated by default on-the-fly ultrasoft pseudopotentials (USP) and reciprocal space integration was conducted with the Monkhorst-Pack sampling scheme, with a minimum of a $2 \times 2 \times 2$ *k*-point grid.[36, 37] Variable cell geometry optimisations were executed with the Broyden-Fletcher-Goldfarb-Shanno (BFGS) minimisation algorithm and the following parameters: (i) a precise basis set; (ii) maximum geometry force and stress tolerances of 0.02 eV $Å^{-1}$ and 0.02 GPa, respectively; (iii) an electronic energy tolerance of 2.0×10^{-6} eV; (iv) a geometry energy tolerance of 1.0×10^{-5} eV; and (v) a maximum ionic displacement criterion of 0.001 Å. No symmetry constraints were imposed upon any structure during optimisation. Energy-volume landscapes were obtained by subjecting each optimised structure to a range of isotropic tensile and compressive stresses.

Ab initio calculations on all molecular species were carried out with the GAUSSIAN09 suite of programs[38] using second-order Møller-Plesset perturbation theory (MP2) and a split-valence triple-zeta basis set 6-311++G(d,p), with supplementary d-type polarisation functions on all main-group elements, p-type polarisation functions on hydrogen and diffuse functions on all atoms. Minimum energy structures on the potential energy surface were located using the Berny algorithm and verified by the absence of negative eigenvalues in the diagonalised Hessian matrix. Angular bending potentials were obtained *via* relaxed potential energy surface scans of the B-O-B bridging angle; in each case the HB-OB/BO-BO torsion angle was constrained to a specified value, whilst all other internal coordinates were fully optimised at each stage. All calculations were conducted *in vacuo*. Natural bond orbital (NBO) analyses[39] were conducted on the MP2 optimised structures.

Localised geometric simulations were conducted with the GASP program[40] in order to identify the flexibility windows of the B_2O_3-I and B_2O_3-IR frameworks, windows within which the rigid trigonal BO_3 units or 'clusters' remain undistorted from their idealised geometries. Geometric simulations model the bonding within relatively rigid units such as BO_3 by a template which represents the ideal bonding geometry of the cluster. Harmonic constraints which connect each atom to the corresponding vertex of a template impose

energetic penalties if there is any deviation from the ideal cluster geometry. During a geometric simulation, atom and template positions are varied by minimising deviations from cluster geometry and the steric overlap of atomic spheres. This cheap geometric technique is quite different from *ab initio* or traditional atomistic potential methods. Energy landscapes are not generated but it is possible to investigate cheaply framework geometries for large systems that satisfy local steric and bonding geometric constraints. Here simulations were carried out with an oxygen hard-sphere radius of 1.350 Å and B–O bond lengths of 1.390 Å, in accordance with the bond lengths returned by *ab initio* calculations on the B_2O_3 structure. Default mismatch and minimum move criteria were implemented in all simulations, with geometric relaxation deemed to be successful if the largest disparities between the relaxed and idealised template structures remained lower than 0.001 Å for B-O bond lengths and 0.001˚ for O-B-O bond angles. The flexibility window is defined as the range of 'framework volumes' over which the BO_3 units which make up the framework can in principle be made geometrically ideal.

Coordination and angular flexibility

In the two experimentally known crystalline B_2O_3 polymorphs – B_2O_3-I and B_2O_3-II – adjacent boron atoms are coupled by an intermediate oxygen atom, forming an interlinked network of B-O-B bridges. The flexibility of these simple frameworks is significantly different, as can be seen by contrasting the energy-volume profiles of B_2O_3-I and B_2O_3-II (Figure 3). The energy landscape of B_2O_3-I is considerably broader than that of the high-pressure B_2O_3-II polymorph.

In this paper, we quantify the width of the energy-volume landscapes, as measured by the maximum and minimum volumes, V_5^{Max} and V_5^{Min} respectively, at 5 kJ mol^{-1} above the local minimum, by the dimensionless parameter ξ_5:

$$\xi_5 = \frac{V_5^{Max} - V_5^{Min}}{V_5^{Min}} \quad (1)$$

The energy of B_2O_3-I varies by only 5 kJ mol^{-1} over a wide volume range 8.0 – 14.6 Å^3 atom^{-1} (ξ_5=0.83), while the B_2O_3-II polymorph is far more rigid, with a corresponding range of only 6.8 – 8.6 Å^3 atom^{-1} (ξ_5=0.26).

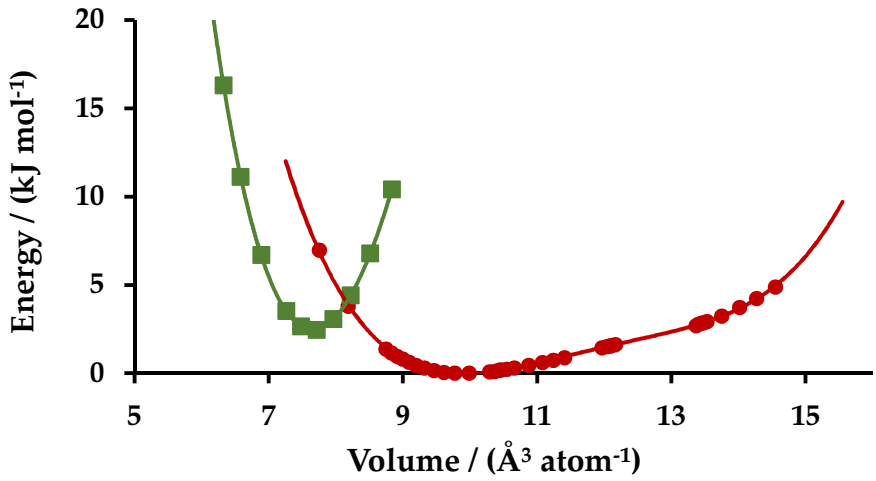

Figure 3: Energy-volume profiles for B_2O_3-I (●) and B_2O_3-II (■).

These polymorphs differ in two fundamental respects: the density of B-O-B linkages, which is higher for B_2O_3-II, and the coordination of the boron atoms (3 for B_2O_3-I, 4 for B_2O_3-II). The former confers topological rigidity, whilst the latter dictates the angular flexibility of each individual bridge. Both contribute to the relative widths of the energy landscapes for B_2O_3-I and B_2O_3-II.

To examine bridge flexibility, we consider the angular bending potentials of two equivalent molecular systems. To reflect the presence of the trigonal BO_3 clusters in B_2O_3-I, the simple boroxane H_2B-O-BH_2 was selected as the molecular analogue. In order to retain the bonding character but with tetrahedral coordination, the corresponding dianion $[H_3B$-O-$BH_3]^{2-}$ was employed to represent a B-O-B bridge in B_2O_3-II. As in previous studies, two equilibrium structures were identified for H_2B-O-BH_2: one has C_{2v} symmetry and an optimised B-O-B bond angle of 123°, and the second D_{2d} symmetry with an angle of 180° (Figure 4).[41,42] The two structures are similar in energy, with calculations at the MP2/6-311G++(d,p) level confirming the C_{2v} structure as the global minimum on the potential energy surface. The fully extended planar conformation has D_{2h} symmetry and corresponds to a second-order stationary point on the potential energy surface; this species is 42.9 kJ mol^{-1} less stable than the equilibrium D_{2d} structure and lies 48.4 kJ mol^{-1} above the global minimum.

A single minimum was characterised on the potential energy surface of $[H_3B\text{-}O\text{-}BH_3]^{2-}$; the corresponding eclipsed structure is of C_{2v} symmetry, and also has an optimised B-O-B bond angle of 123°.

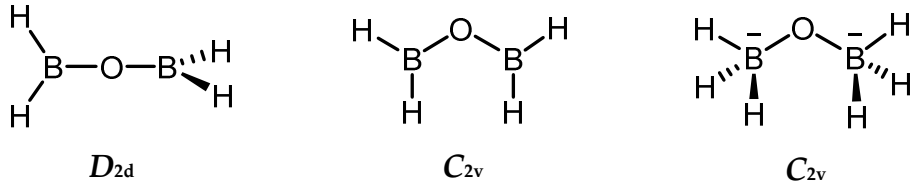

Figure 4: Equilibrium structures for $H_2B\text{-}O\text{-}BH_2$ and $[H_3B\text{-}O\text{-}BH_3]^{2-}$, calculated at the MP2/6-311++G(d,p) level of theory. The C_{2v} structure of $H_2B\text{-}O\text{-}BH_2$ is the global minimum on the PES, lying 5.5 kJ mol^{-1} below the optimised D_{2d} structure.

The potential energy of the $H_2B\text{-}O\text{-}BH_2$ molecule as a function of the B-O-B bond and HB-OB torsion angles is shown in Figure 5. The bending potential in $H_2B\text{-}O\text{-}BH_2$ is highly dependent upon the angle between the two BH_2 planes. Compressing the B-O-B linkage in the D_{2d} structure (HB-OB = 90˚) lowers the symmetry to C_s and the energy increases; in contrast, a reduction in the B-O-B angle from 180° in the C_{2v} structure (HB-OB = 0˚) leads to an energy minimum at 123°.

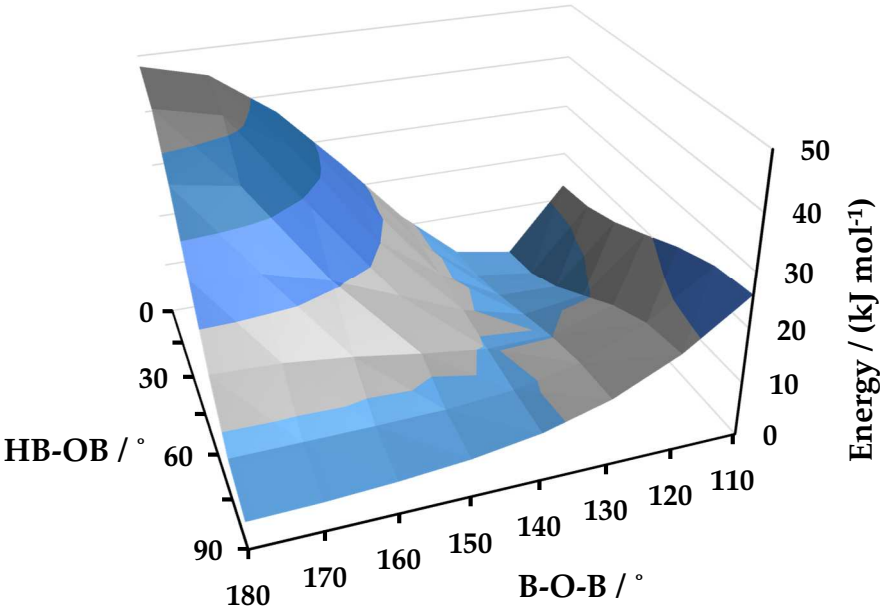

Figure 5: Potential energy surface of $H_2B\text{-}O\text{-}BH_2$, plotted as a function of the B-O-B bond angle (110˚ – 180˚) and the HB-OB torsion angle (0˚ – 90˚). The C_{2v} structure corresponds to HB-OB = 0˚ and the D_{2d} structure to HB-OB = 90˚. All other internal coordinates were fully optimised at each point.

Starting from the global minimum C_{2v} structure, to achieve B-O-B angles greater than 135° without surmounting a significant potential energy barrier, there must be a concurrent increase in the HB-OB torsion angle (Figure 5) – beyond B-O-B angles of 135°, the structure can be stabilised by abandoning planarity and deforming towards the staggered C_s structure. Thus, cooperation between bending and twisting motions of the bridge is crucial for its facile compression and expansion; provided there is complete torsional freedom, the B-O-B bond angle can vary between 110° and 180° with a minimal change in energy (< 10 kJ mol^{-1}). Without torsional freedom, the B-O-B linkage is far more rigid.

The subtle balance in energy between the two equilibrium structures is a fundamental feature of the B-O-B bridge, and can be readily explained by valence bond theory.[43] A number of plausible resonance forms are readily available for H_2B-O-BH_2 (Figure 6). A natural bond orbital analysis of the MP2 optimised equilibrium structures suggests that the resonance structure that accounts most comprehensively for the total electron density (ρ_{Lewis} = 0.997) incorporates a three-centre bonding orbital $\tau_{B\text{-}O\text{-}B}$, derived from the normalised linear combination of an oxygen 2p orbital and parallel 2p orbitals from each of the adjoining boron atoms. Each B-O bond is also described by a $\sigma_{B\text{-}O}$ bonding orbital, while the central oxygen atom maintains an occupied valence nonbonding orbital n_o of hybridisation $sp^{3.86}$. The analysis also suggests that the D_{2d} structure of H_2B-O-BH_2 is most accurately represented (ρ_{Lewis} = 0.995) by the doubly-bonded resonance form, which resembles the isoelectronic molecule allene (Figure 6). Each of the two equivalent B-O interactions is best described by two bonding NBOs – $\sigma_{B\text{-}O}$ and $\pi_{B\text{-}O}$ – which are heavily polarised towards the bridging oxygen.

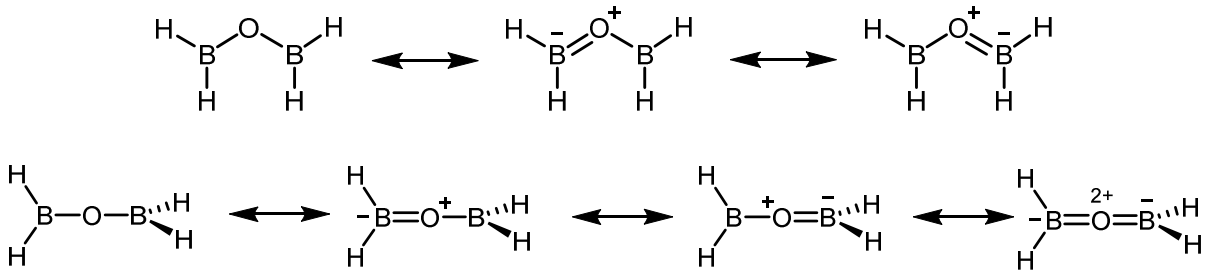

Figure 6: Resonance forms for the C_{2v} and D_{2d} structures of H_2B-O-BH_2. Formally the π-bonding in the D_{2d} species consists of two $\pi_{B\text{-}O}$ bonding orbitals; in the C_{2v} structure it is best described by a single three-centred bonding orbital $\tau_{B\text{-}O\text{-}B}$.

Table 1 summarises the key structural parameters, including the length and Wiberg bonding indices (WBI) of the B-O bonds and the natural charge distribution, of the two equilibrium structures of H_2B-O-BH_2.

Structure	B-O-B angle / °	B-O length / Å	B-O WBI	Q(B) / *e*	Q(O) / *e*	$L_{H\text{-}H}$ / $2r_H$
C_{2v}	123	1.378	0.837	0.801	-0.985	1.03
D_{2d}	180	1.345	0.862	0.801	-0.985	1.71

Table 1: Key structural parameters for the two equilibrium structures of H_2B-O-BH_2, including the B-O-B bond angle, lengths and Wiberg bonding indices (WBI) of the B-O bonds and the natural charge distribution. Q(B) and Q(O) are natural charges and $L_{H\text{-}H}$ denotes the closest through-space H-H separation in each species. r_H is the van der Waals radius of hydrogen.

The key point is that although conjugation is more extensive in the D_{2d} structure – as shown by the shorter B-O bond length (1.345 Å, *vs*. 1.378 Å for the C_{2v} structure) and larger Wiberg bonding index (0.862 *vs*. 0.837) – its stabilising influence is compensated by the hybridisation of the valence nonbonding orbital n_o in the C_{2v} structure.

Central to the flexibility of H_2B-O-BH_2 is the presence of three-coordinate boron. The bending potential of the B-O-B bridge in $[H_3B\text{-}O\text{-}BH_3]^{2-}$, where boron is four-coordinate, is instead characterised by a relatively deep well for all HB-OB torsion angles. Figure 7 shows the bending potential for the eclipsed C_{2v} structure. Increasing the coordination of boron from three to four removes the lone vacant 2p orbital from the system, prevents pπ-donation from the bridging oxygen and stiffens the B-O-B bridge. This provides a rationalisation of the very different flexibilities of B_2O_3-I and B_2O_3-II shown in Figure 3.

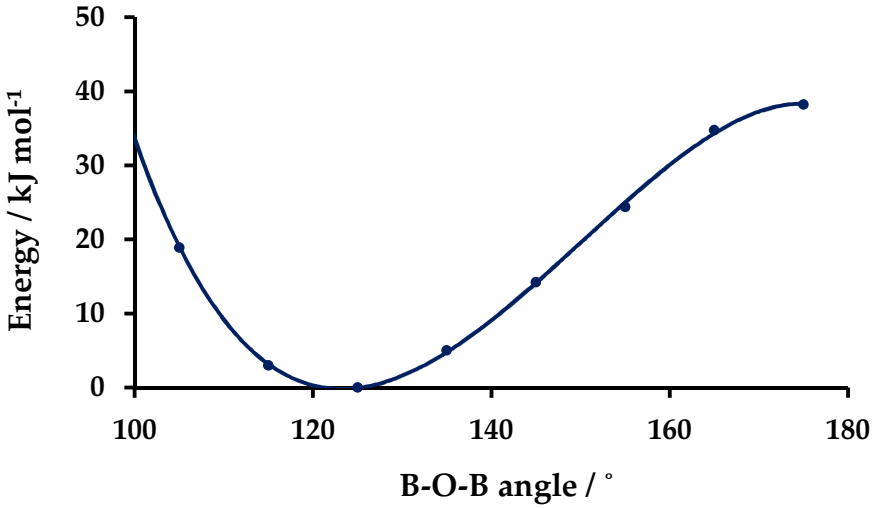

Figure 7: Bending potential for the C_{2v} structure of $[H_3B\text{-}O\text{-}BH_3]^{2-}$, obtained from a relaxed potential energy scan of the B-O-B angle at fixed symmetry (HB-OB = 0°).

Coordination and topological rigidity

The trigonal coordination of boron in B_2O_3-I, compared with the tetrahedral coordination in B_2O_3-II, changes not only the B-O-B bending potential but also the *topological freedom* in the structure, i.e. the density of B-O-B linkages. To decouple these two effects, it is necessary to compare structures with similar bending potentials but containing atoms with different valencies and hence coordinations. To achieve this, we turn our attention to β-cristobalite. This cubic polymorph of silica comprises an interlinked network of rigid SiO_4 tetrahedra connected by Si-O-Si bridges. The silicon atoms are four-coordinate, as in B_2O_3–II, yet the energy-volume landscape is considerably broader. Under the 5 kJ mol^{-1} ceiling defined earlier, the volume occupied per atom varies between 12.6 – 18.6 $Å^3$ $atom^{-1}$ ($\xi_5 = 0.48$). Similar flexibility is present in a range of silicate frameworks.[44,45] As for B_2O_3-I, the origin of this flexibility may be traced to the angular bending potential of a simple molecular analogue, $H_3Si\text{-}O\text{-}SiH_3$, which is compared with that of $H_2B\text{-}O\text{-}BH_2$ in Figure 8. Like $[H_3B\text{-}O\text{-}BH_3]^{2-}$, the bending potential is essentially independent of the HSi-OSi torsion angle, but like the C_s species of $H_2B\text{-}O\text{-}BH_2$ it is exceptionally flat over the range 120˚ – 180˚, with a very shallow minimum at 155˚. As a consequence of the flexibility of the Si-O-Si linkage, a wide range of bridging bond angles have been observed experimentally in many different silicate frameworks.[45,46,47]

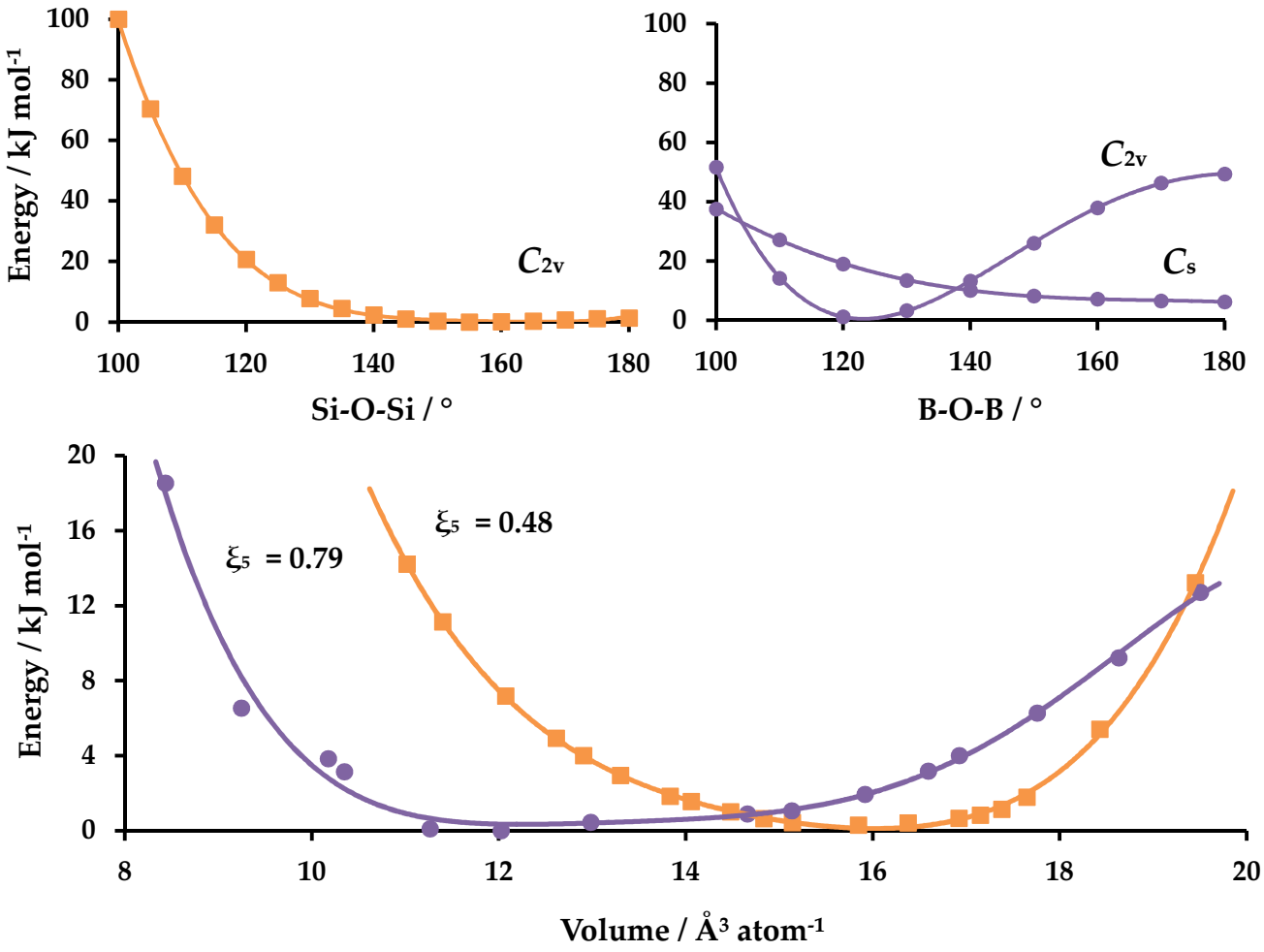

Figure 8: Upper frames: Molecular bending potentials of $H_3Si\text{-}O\text{-}SiH_3$ (■) and $H_2B\text{-}O\text{-}BH_2$ (●); the two profiles for $H_2B\text{-}O\text{-}BH_2$ correspond to the C_s and C_{2v} structures. Lower frame: Plane-wave DFT energy-volume landscapes of β-cristobalite (■) and β-cristobalite-borate-a (●), in which B_2O_5 units have replaced all the SiO_4 tetrahedra, as described in the text

Given any arrangement of SiO_4 tetrahedra, it is possible to construct a related structure in which the SiO_4^{4-} tetrahedra are exchanged for $B_2O_5^{4-}$ units and all B atoms are three-coordinate. For each tetrahedron, there are three ways in which such a substitution can be realised, since the B-B axis can be aligned along any one of the three tetrahedral C_2 axes.

The DFT energy landscape of β-cristobalite-borate-a (β-CB-a), obtained by making such a substitution and orienting all the B-O-B bridges along the *a*-axis, is superimposed upon that of the silicate precursor in Figure 8. The energy landscape of β-CB-a is notably broader than its silicate precursor, covering a volume span of 9.7 – 17.4 $Å^3$ $atom^{-1}$ with an energy change < 5 kJ mol^{-1} (ξ_5 = 0.79). More subtle is the change in the form of the energy landscape; while for β-cristobalite the minimum energy structure lies towards the high volume end of the flexible region, for the borate-analogue it resides towards the low volume end. This is consistent with the findings of Wells *et al.*[40,44], who have explored the notion of flexibility windows in zeolites and other covalent frameworks and observed that silicates exhibit an atypical tendency to be maximally extended in their relaxed states. This correlates with the absence of any local minimum at small angles in the $H_3Si\text{-}O\text{-}SiH_3$ bending potential (Figure 8).

The replacement of SiO_4^{4-} tetrahedra by $B_2O_5^{4-}$ units should produce little change in the angular flexibility of the polyhedral bridges – in fact, depending on how twisted the bridges are, such a substitution may rigidify the structure – but the energy-volume landscape widens nevertheless. As such, we conclude that it is unwise to focus entirely on bending potentials, for it is apparent that topological freedom also dictates the flexibility of covalent frameworks.

A vast array of theoretical B_2O_3 polymorphs may be obtained from silicates in this manner, including new families of zeolites, and we expect the changes observed for β-cristobalite will be general. It is important to stress also that the β-cristobalite-borate-a structure is almost isoenergetic with the experimental B_2O_3-I polymorph (higher in energy by less than 0.2 kJ mol^{-1}).

Exploring flexibility in B_2O_3-I and B_2O_3-IR

Although the energy landscape of the crystalline B_2O_3-I polymorph has been reported previously[24], there has been no examination of the structural transformations observed during the expansion and compression of the framework. Below a ceiling of 5 kJ mol^{-1}, the volume of the B_2O_3-I unit cell is free to vary from 8.0 – 14.6 $Å^3$ (ξ_5 = 0.83), with the *a*-lattice parameter varying only in the range 4.2 – 4.6 Å while the *c*-parameter varies over a much wider range of 7.7 – 11.8 Å. The B_2O_3-I framework is thus inherently anisotropic in its flexibility, with the shallow region of the energy landscape dominated by the expansion and compression of the framework along the *c*-axis. During the expansion of B_2O_3-I, a barrierless pressure-induced transition is observed between -1.5 and -1.6 GPa; this transition leads to a substantial anisotropic decompression of the framework along [001] and regular hexagonal channels of diameter 4.5 Å form, aligned along the same direction. The pleated ribbons of trigonal BO_3 units undergo a significant reconfiguration to form, as viewed along the [001] direction, a series of interlocking planar sheets (Figure 9). This expanded structure is very similar to the theoretical polymorph B_2O_3-0, first proposed by Huang and Kieffer on the basis of molecular dynamics simulations[48].

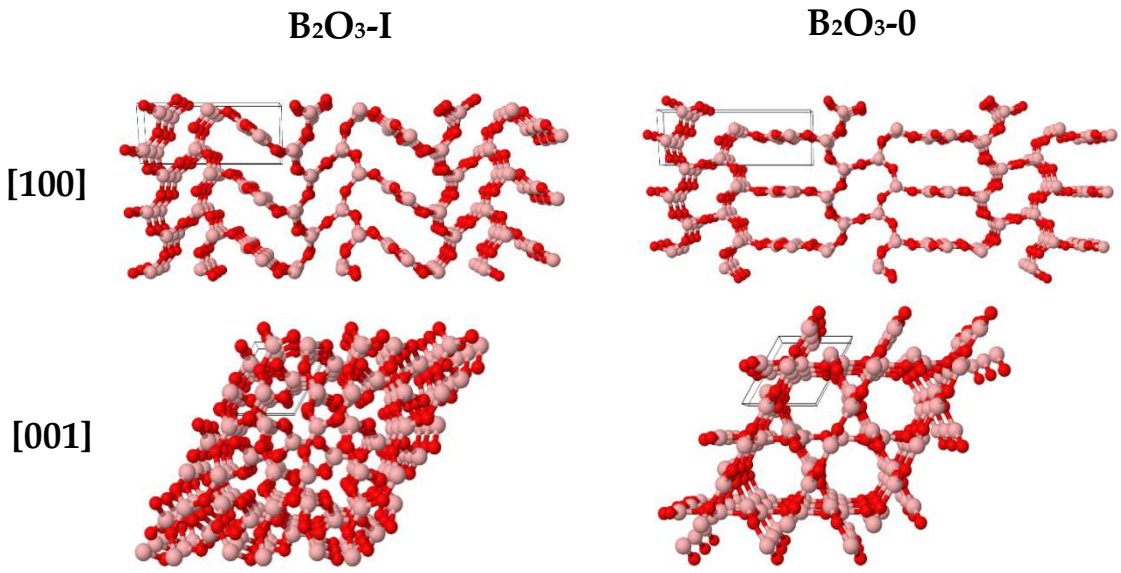

Figure 9: Optimised structures for the two polymorphs B_2O_3-I and B_2O_3-0, viewed along the [100] and [001] directions. Boron atoms here and in subsequent figures are pink; oxygen atoms are dark red. Black lines show the unit cells.

The B_2O_3-I unit cell contains nine distinct B-O-B bridges, which can be classified into a set of three and a set of six according to their behaviour over the energy landscape. Figure 10 shows that the group of six bridges are part of almost planar B_2O_5 units and exhibit B-B vectors with significant components perpendicular to the [001] direction; the group of three bridges are part of highly twisted B_2O_5 units, as is also clear from Figure 10, and have B-B vectors with significant components parallel to [001].

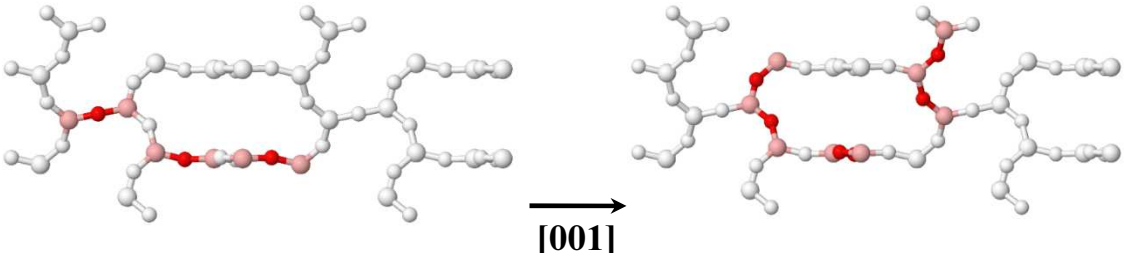

Figure 10: B_2O_3-I framework, highlighting the two distinct groups of B-O-B bridges. The left figure depicts the three B_2O_5 units that undergo twisting towards the staggered C_s conformation as the framework expands; the figure on the right depicts the six B_2O_5 units that do not undergo any significant twisting during structural expansion.

During the expansion of the framework, the B_2O_5 units containing the set of six bridges retain their planarity, with the bridge angles expanding from an average of 125.8˚ at the low volume end to 145.6˚ at the high volume end; the group of three bridges, however, undergo a much greater extent of decompression from 129.5˚ to 163.5˚ and distort further towards the staggered C_s conformation, with the OB-OB torsion angle increasing over the range 43.1˚ – 58.8˚. This suggests that these twisted B_2O_5 units are integral to the anisotropic flexibility of the B_2O_3-I framework, and moreover that the torsional freedom of the bridges in these units should dictate the flatness of the energy-volume landscape.

As emphasised in the introduction, boron atoms and boroxyl rings (B_3O_3) are interchangeable structural units in B_2O_3 frameworks, for their substitution preserves the stoichiometry of the compound, the coordination state of boron and the underlying topology. In particular, Figure 1b shows how the boroxyl-decorated B_2O_3-I framework (A-R in Figure 1 and ref. 22 or, equivalently, B_2O_3-IR) is characterised by an exceptionally broad energy landscape. For the predefined ceiling of 5 kJ mol^{-1}, the volume of the unit cell if free to vary from 10.6 – 45.2 Å^3 atom^{-1} (ξ_5 = 3.26); this is approximately four times broader than B_2O_3-I (ξ_5 = 0.83) and more than an order of magnitude broader than B_2O_3-II (ξ_5 = 0.26).

The structural transformations of B_2O_3-IR under tensile and compressive stresses emulate that of its precursor, but the magnitude of the changes are considerably larger. Over the shallow region (< 5 kJ mol^{-1}) of the energy landscape: (i) the *a*-lattice parameter varies by a relatively small amount between 8.3 – 9.8 Å, while the *c*-lattice parameter varies much more, between 7.9 – 24.6 Å; (ii) the set of six bridges that are part of planar B_2O_5 units expand from 123.5˚ to 179.4˚; and (iii) the set of three bridges that are part of twisted B_2O_5 units expand from 121.3˚ to 179.4˚, twisting significantly from an OB-OB torsion angle of 26.1 to 58.1˚. As before, a pressure-induced phase transition precipitates the formation of hexagonal channels coincident with the [001] direction (Figure 11). We denote this low-pressure boroxyl-decorated phase B_2O_3-0R, by analogy[22] with B_2O_3-0. Ferlat *et al.*[17] discounted the B_2O_3-0 phase as insignificant in explaining the ready vitrification of boron oxide, citing both its high energy and the absence of boroxyl rings; B_2O_3-0R cannot be so dismissed for our calculations indicate it is essentially isoenergetic with B_2O_3-I.

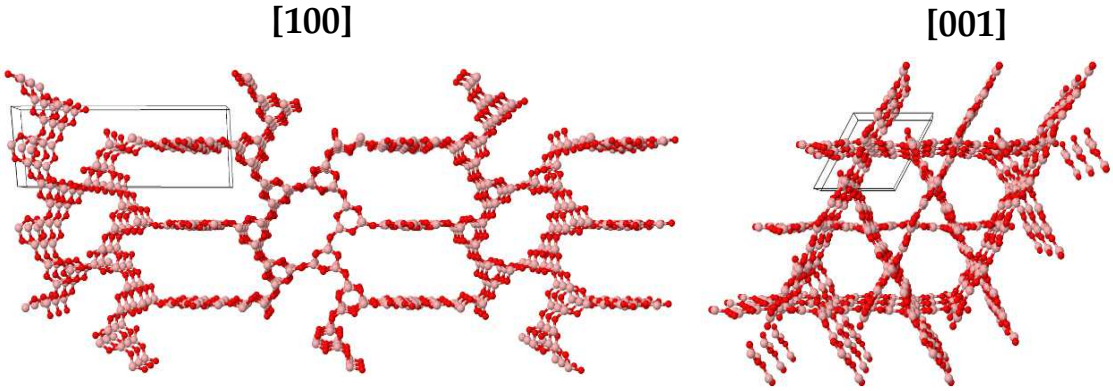

Figure 11: Optimised structure of the B_2O_3-0R framework, as viewed along the [100] and [001] directions. Black lines show the unit cells.

Understanding and tuning structure flexibility

Several proposals have been made previously to account for the vastly increased flexibility of B_2O_3-IR, the boroxyl-decorated analogue of the B_2O_3-I framework[24]. One possibility is that when boroxyl rings are incorporated in the framework, each boron atom is now involved in only one flexible B-O-B bridge – with the other two neighbouring oxygens confined to the B_3O_3 ring with fixed O-B-O angles. In contrast, in B_2O_3-I each boron atom is surrounded by flexible bridges in all directions. A further suggestion is that extended π-conjugation in the boroxyl-decorated frameworks could influence the angular flexibility of the bridging linkages.

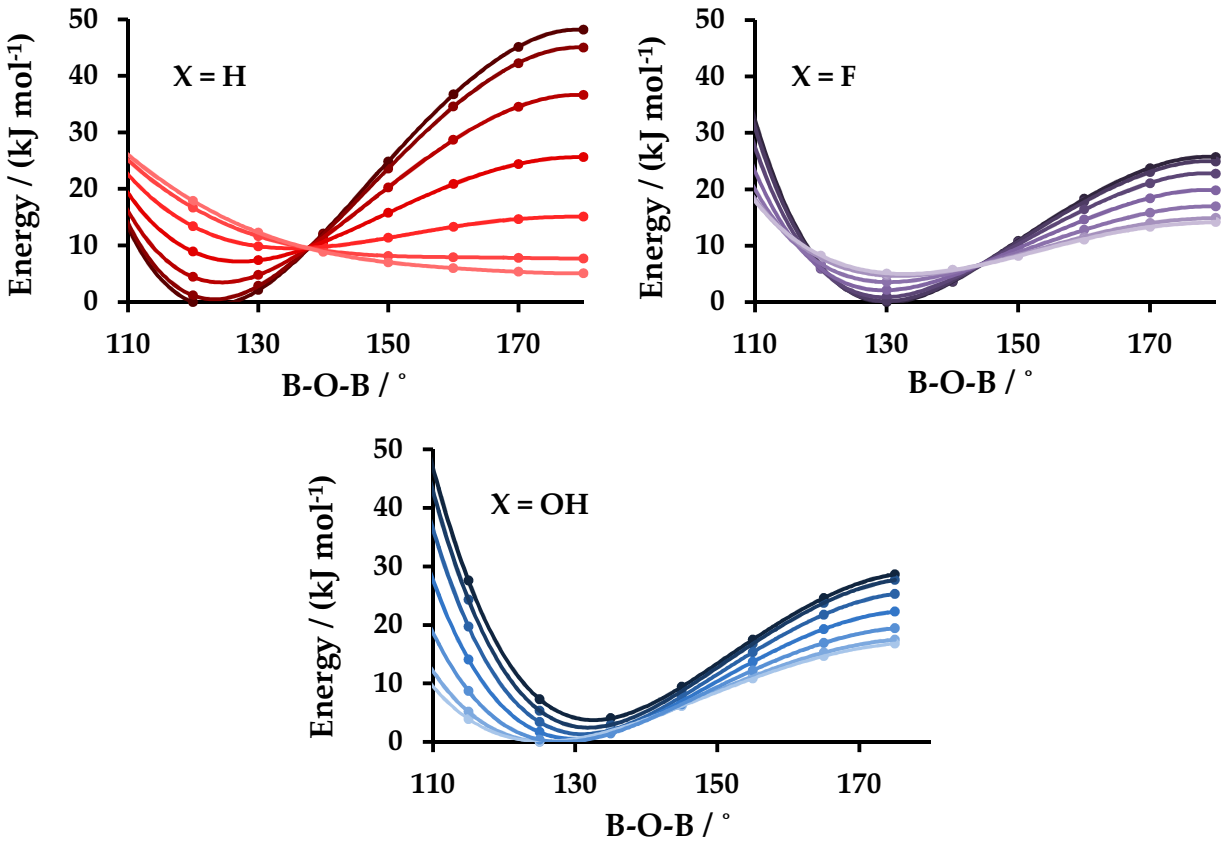

Figure 12: Bending potentials of X_2B-O-BX_2 (X = H, F, OH). In each case the top curve defines the bending potential for the planar C_{2v} conformation (XB-OB = 0˚) and the lowest curve the staggered C_s conformation (XB-OB = 90˚); the intermediate curves correspond to the B-O-B bending potentials at XB-OB torsion angle intervals of 15˚.

To test which of these two factors is more important, Figure 12 compares bending potentials for X_2B-O-BX_2 where X = H, F and OH. The cooperativity between the B-O-B bridging angle and XB-OB torsion angle present in H_2B-O-BH_2 is damped in both F_2B-O-BF_2 and $(HO)_2$B-O-B$(OH)_2$, due to competing pπ-pπ* donor-acceptor interactions from the peripheral heteroatoms. The angular bending potential of the B-O-B bridge in the boroxyl analogue $(B_3O_3H_2)$-O-$(B_3O_3H_2)$ (Figure 15) emulates that of $(HO)_2$B-O-B$(OH)_2$ almost exactly. Similar interactions and angular flexibility are observed in $(B_3O_3H_2)$-O-$(C_3N_3H_2)$) (Figure 15) and $(B_3N_3H_5)$-O-$(B_3N_3H_5)$ (Figure 16), indicating that provided heteroatom X has an available lone pair it can compete effectively with the bridging oxygen for the lone vacant 2p orbital on boron.

Further calculations were conducted on B$(OBH_2)_3$ and the boroxyl-analogue $(B_3O_3)(OBH_2)_3$. In B$(OBH_2)_3$, the central boron atom is involved in three flexible bridges, whereas in $(B_3O_3)(OBH_2)_3$ each endocyclic boron is in just one flexible bridge. These two molecules thus allow us to examine whether the fixed O-B-O bond angles in the boroxyl system enhance, diminish or leave unaffected the flexibility of the bridges. In each system the three B-O-B bridges were expanded concurrently over the range 120-175˚; this was repeated for five torsional configurations – triplanar (T), diplanar (D), monoplanar (M), non-planar (N) and perpendicular (P) –(Figure 13). The bending potentials for B$(OBH_2)_3$ and $(B_3O_3)(OBH_2)_3$ exhibit only very minor differences between the five configurations, showing that whether each boron atom is involved in one or three flexible bridges is immaterial.

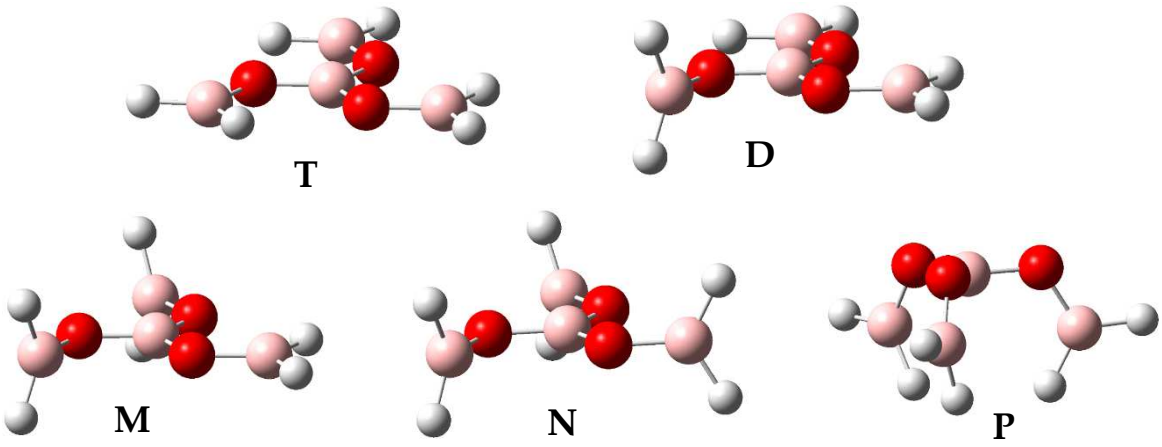

Figure 13: The five torsional configurations (T, D, M, N and P) studied for $B(OBH_2)_3$ and $(B_3O_3)(OBH_2)_3$. In each case, all three bridges were expanded simultaneously with fixed HB-BO torsion angles. The energy changes are essentially identical in the two molecules, proving that the bending potential of one B-O-B bridge depends only upon the geometry of the local B_2O_5 unit and not upon the configuration of any neighbouring bridges.

Thus, in general, molecular calculations reveal that there is no intrinsic difference between the electronic structure of the bridges in B_2O_3-I and B_2O_3-IR: on the contrary, the angular flexibility of the bridge appears to be governed exclusively by the geometry of the local B_2O_5 unit (i.e., O_2B-O-BO_2) and *not* by any longer range electronic effects.

In the absence of any significant differences in the electronic structures of the bridges, the enhanced flexibility of B_2O_3-IR relative to B_2O_3-I must therefore be geometric or topological in origin. Exchanging boron atoms for boroxyl rings increases the diameters of the framework cavities at high volumes, reduces the number density of B-O-B bridges and increases the number of bonds between neighbouring bridging oxygens by separating them with a rigid spacer. We suggest that these features increase the torsional freedom of the bridges and their independence within the framework. Across all of the B_2O_3 structures considered here and in ref. 24, there is a very strong inverse correlation, shown in Figure 14, between the number density of flexible B-O-B bridges, $N_{B\text{-}O\text{-}B}$, in the optimised structure and

the width of the energy-volume landscape, as measured by the dimensionless parameter ξ_5 (defined in equation (1)).

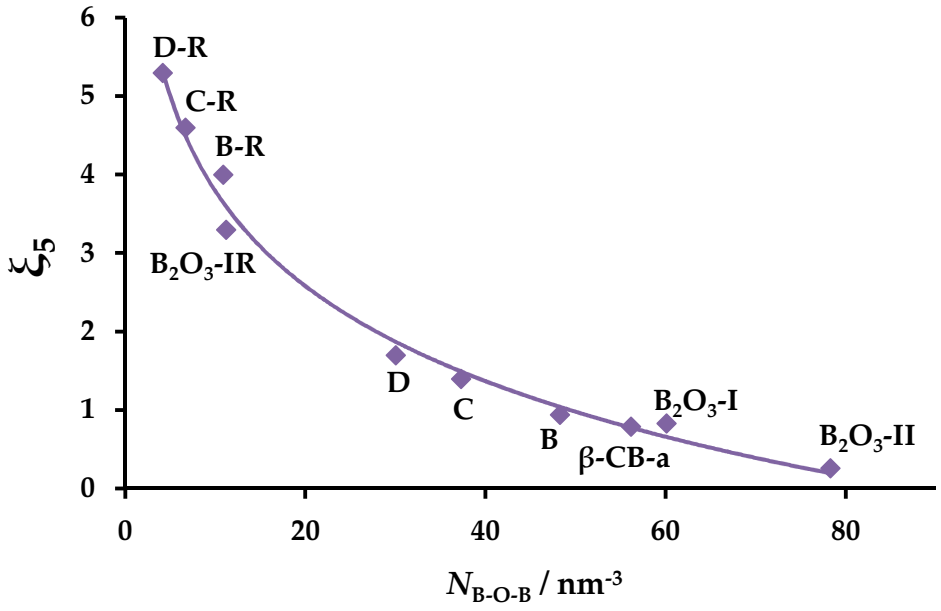

Figure 14: The width ξ_5 (defined in equation (1)) of the energy landscape 5 kJ mol^{-1} above the local minimum as a function of the number density of flexible B-O-B bridges ($N_{\text{B-O-B}}$) in each of the polymorphs considered to-date. Structures B/B-R, C/C-R and D/D-R were reported in ref. 24. There is a very strong inverse correlation, suggesting that the extreme energy-volume landscapes of the boroxyl-decorated polymorphs may be simply ascribed to their very low density of B-O-B bridging linkages.

Although such an analysis is informative, in reality these frameworks are networks of interlinked bridges. During expansion and compression of the framework, the bridges cannot deform according to their individual preference, but instead are obliged to distort collectively. The manner in which the bridges are connected, and not simply their density, should therefore modulate the flexibility. It is also entirely plausible that the boroxyl rings serve principally as physical spacers between the bridges, offering additional degrees of torsional freedom absent from the B_2O_3-I structure; in frameworks without boroxyl rings, the closest

pairs of bridging oxygen atoms are separated by two bonds, as opposed to four bonds in exclusive boroxyl systems.

If these topological factors dominate, the frameworks containing boroxyl rings should retain a significant proportion of their flexibility if other six-membered rings replace boroxyl. We therefore consider a range of frameworks obtained by decorating the B_2O_3-IR system with isoelectronic six-membered rings – namely, triazine, borazine and benzene – whilst retaining the bridging oxygen atoms.

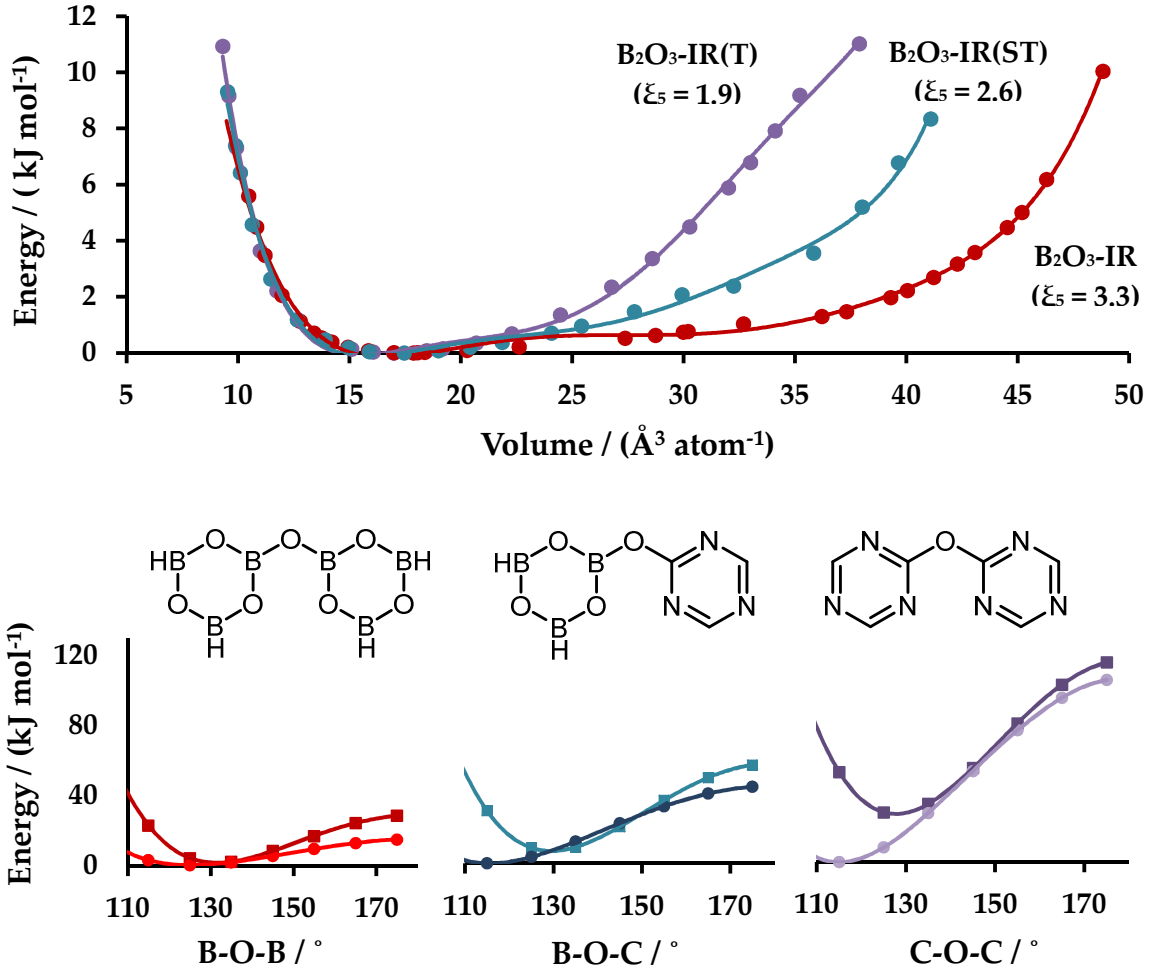

Figure 15: Bending potentials of $(B_3O_3H_2)$-O-$(B_3O_3H_2)$, $(B_3O_3H_2)$-O-$(C_3N_3H_2)$ and $(C_3N_3H_2)$-O-$(C_3N_3H_2)$ and energy landscapes of the corresponding decorated B_2O_3-IR frameworks. The two bending potentials correspond to the planar C_{2v} conformation (■) and the staggered C_s conformation (●)

Exchanging all the boroxyl rings for triazine yields a framework with C-O-C bridges (B_2O_3-IR(T)), whilst replacing alternate boroxyl rings with triazine (B_2O_3-IR(ST)) generates an interlinked network of B-O-C bridges. The corresponding energy landscapes of B_2O_3-IR,

B_2O_3-IR(T) and B_2O_3-IR(ST) are depicted in Figure 15, alongside the planar and staggered bending potentials of their molecular analogues.

The molecular bending potentials show that the angular flexibility of the bridge varies in the order B-O-B > B-O-C > C-O-C, with the well depths increasing more than two-fold with each boron-carbon substitution. This likely reflects the weakening of pπ-pπ* donation from the bridging oxygen into the rings and the increasing dominance of the valence nonbonding orbital on oxygen. At small volumes, the three energy-volume profiles are superimposable almost exactly, suggesting that further compression is prohibited exclusively by the topology of the structure and not at all by the bridge flexibility. It is clear, nevertheless, that the bending potential of the bridge governs the capacity of the framework to undergo expansion, with the widths of the energy well decreasing significantly as the triazine content increases. In B_2O_3-IR(ST), over the volume range defined by $\xi_5 = 2.6$, the bridge angles in the six planar B_2O_5 units vary over the range 122.9˚ – 146.6˚ and the bridge angles in the three twisted B_2O_5 units vary over the range 116.2˚ – 145.1˚; in B_2O_3-IR(T) ($\xi_5 = 1.9$), the analogous ranges, 124.4˚ – 137.1˚ and 115.4˚ – 137.5˚ respectively, are narrowed at the upper volume limit of the ξ_5 region, . The nature of expansion in both B_2O_3-IR(ST) and B_2O_3-IR(T) is the same as in B_2O_3-IR, with the emergence of hexagonal channels along the [001] direction at high volumes. While making the bridges more rigid appears to have a significant impact upon the flexibility of the B_2O_3-IR framework, it is important to note that the energy landscapes remain considerably broader than that of the B_2O_3-I framework.

Frameworks constructed from borazine and benzene – abbreviated to B_2O_3-IR(Bo) and B_2O_3-IR(Be), respectively – exhibit similar trends in flexibility, as demonstrated in Figure 16. The presence of clashing *ortho*-hydrogens, however, hinders torsional rotations in the $B_3N_3H_5$ and C_6H_5 units, leading to structures with larger optimised volumes and a reduced capacity for compression. In B_2O_3-IR(Be), the bridges expand from 109.4˚ – 138.3˚ over the ξ_5 region, whereas in B_2O_3-IR(Bo) the bridge angles increase up to 179.3˚ at the high-volume limit.

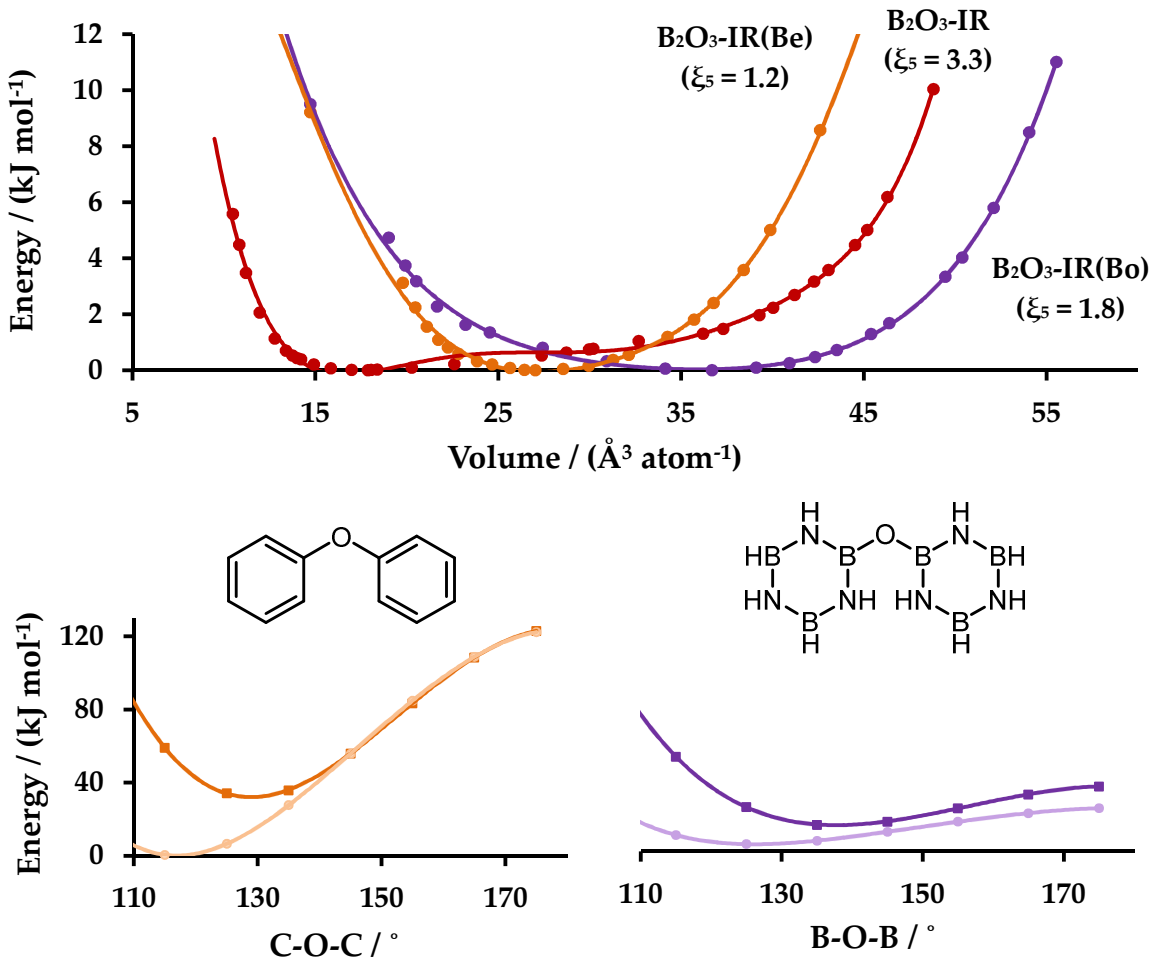

Figure 16: Bending potentials of (C_6H_5)-O-(C_6H_5) and $(B_3N_3H_5)$-O-$(B_3N_3H_5)$ and energy landscapes of the corresponding decorated B_2O_3-IR frameworks. As in Figure 15 the energy landscape of B_2O_3-IR is also shown (red curve). The two bending potentials correspond to the planar C_{2v} conformation (■)and the staggered C_s conformation (●).

The molecular bending potentials of (C_6H_5)-O-(C_6H_5) and $(B_3N_3H_5)$-O-$(B_3N_3H_5)$, shown in Figure 16, follow the trends in angular flexibility outlined above. The structural transformations of the solid-state frameworks B_2O_3-IR(Be) and B_2O_3-IR(Bo) over their energy landscapes, however, differ from B_2O_3-IR. As opposed to undergoing an anisotropic extension along the [001] direction, B_2O_3-IR(Be) and B_2O_3-IR(Bo) extend significantly in all directions. In B_2O_3-IR(Bo), the *a*-parameter varies over the range 6.8 – 10.2 Å and the *c*-

parameter between 21.5 – 25.5 Å, whereas in B_2O_3-IR(Be) the respective ranges are 6.7 – 9.4 Å and 22.1 – 23.3 Å.

Both structures appear incapable of accessing lower *c*-lattice parameters, presumably as the $B_3N_3H_5$ or C_6H_5 units are unable to adopt planar conformations at smaller B-O-B angles due to steric repulsions between *ortho* hydrogens. Despite the significantly rigidified bridges and torsional restrictions, even the energy-volume landscape of B_2O_3-IR(Be) remains wider than B_2O_3-I. The density of bridging linkages is seen to be a fundamental feature in dictating solid-state flexibility.

Sources of flexibility and torsional freedom

The molecular species $(B_3O_3H_2)$-O-$(B_3O_3H_2)$ and $(B_3N_3H_5)$-O-$(B_3N_3H_5)$ have strikingly similar angular flexibilities, yet their corresponding solid-state frameworks B_2O_3-IR and B_2O_3-IR(Bo) behave very differently. B_2O_3-IR(Bo) is far less compressible than B_2O_3-IR because of reduced torsional freedom thanks to clashing ortho-hydrogens. The only significant difference between the two is this torsional freedom of the bridging linkages, and herein may lie another clue to the relative flexibilities of B_2O_3-I and B_2O_3-IR. Figure 17 plots the average OB-OB torsion angle of the set of the three B-O-B bridges contained within twisted B_2O_5 units versus the B-O-B angle for B_2O_3-I and B_2O_3-IR, for all points on the energy landscape below the 5 kJ mol^{-1} ceiling. In both frameworks, the upper limit on the torsion angle is 60˚, as can be seen in the hexagonal channels along the [001] direction; overall, however, there is clearly greater scope for torsional rotations during compression in B_2O_3-IR and torsional freedom can help to explain the differences in flexibility of B_2O_3-I and B_2O_3-IR. Flexibility is due to cooperativity between bending and twisting motions in the bridges during expansion, and this cooperativity requires topological freedom/a low density of bridges.

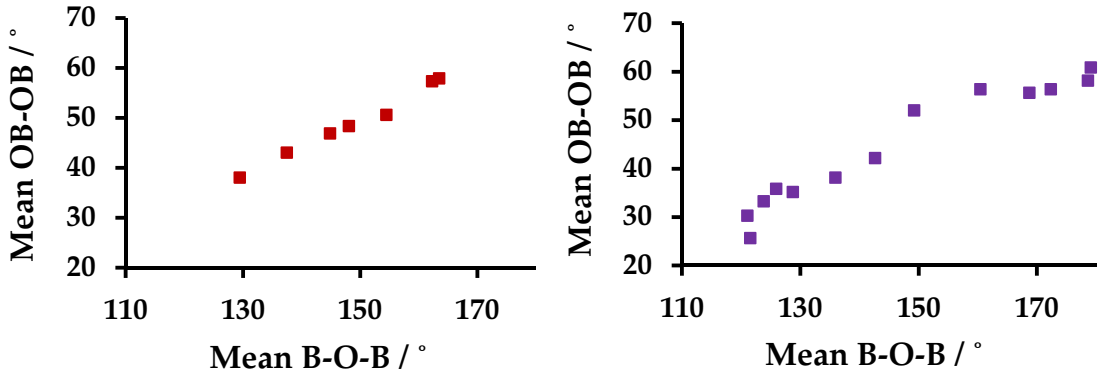

Figure 17: Plots of the mean OB-OB torsion angle versus B-O-B for the three B-O-B bridges contained within the twisted B_2O_5 units present in the unit cells of B_2O_3-I (■) and B_2O_3-IR (■). The lowest and highest angles correspond to the low- and high-volume thresholds of the energy-volume landscapes (5 kJ mol^{-1}), respectively.

The flexibility windows of the B_2O_3-I and B_2O_3-IR frameworks, obtained from template-based geometric simulations, also provide some insight (Figure 18). The flexibility window defines the range of lattice parameters within which the BO_3 units can in principle remain undistorted from their perfect trigonal geometry, and therefore indicates the flexibility intrinsic to a particular framework.

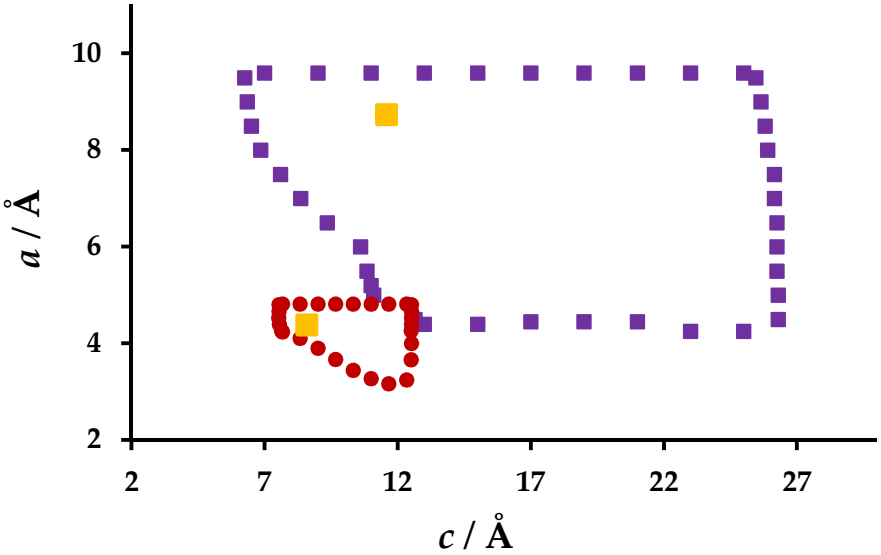

Figure 18: Flexibility windows (*a*-*c*) for B_2O_3-I (●) and B_2O_3-IR (■). The *ab initio* optimised lattice parameters are marked ■. Within the window, the trigonal BO_3 units can retain their ideal geometries, so any changes in volume result from distortions of the flexible B-O-B bridges.

Agreement between the geometric simulations and *ab initio* energy-volume landscapes is remarkably good. The *ab initio* optimised structures of both frameworks reside in the high density region of their flexibility windows – that is, the B_2O_3-I and B_2O_3-IR structures are highly compressed in their relaxed states – in agreement with the presence of a global minimum at small B-O-B angles on the potential energy surfaces of H_2B-O-BH_2, $(OH)_2B$-O-$B(OH)_2$ and $(B_3O_3H_2)$-O$(B_3O_3H_2)$. As anticipated, the window for B_2O_3-IR is considerably larger than for B_2O_3-I: in the broadest regions, the *a*-lattice parameter varies over the range 3.3 – 4.8 Å in B_2O_3-I and 4.3 – 9.6 Å in B_2O_3-IR, while the *c*-lattice parameter is free to vary between 7.6 – 12.5 Å and 6.4 – 26.4 Å, respectively. This verifies the *ab initio* results, proving that the broad energy landscapes in the boroxyl-decorated frameworks are not an

artifact of the DFT calculations.

Two other intriguing features present themselves: (i) for large *a*-parameters, the *c*-axis of the boroxyl-decorated framework can be compressed *further* than B_2O_3-I; and (ii) decorating the B_2O_3-I framework with boroxyl rings alters the profile of the flexibility window. Across the entire window of B_2O_3-I, increasing the *c*-parameter facilitates greater compression along the *a*-axis, whereas in B_2O_3-IR this interplay between lattice parameters is quickly exhausted. In B_2O_3-I, the value of the *c*-lattice parameter restricts the height of the window, suggesting that torsional rotations of the bridges are constrained; in B_2O_3-IR, this only occurs for the smallest values of *c* (< 12 Å).

These simple geometric simulations show that the increased flexibility in B_2O_3-IR is not merely a question of electronics or even the bridge density *per se*: the interdependence of the *a*-*c* lattice parameters is fundamentally different in the two systems, suggesting that intrinsic geometric constraints present in B_2O_3-I are lifted upon decorating the system with boroxyl rings. From a geometric perspective, it is plausible that the increased cavity diameters in B_2O_3-IR permit larger torsional rotations in the framework, affording the B-O-B bridges with degrees of freedom previously unattainable.

Conclusions and final remarks

In this paper we have explored a wide range of low energy boron-oxygen frameworks which exhibit mechanical flexibility unprecedented for purely inorganic materials. We anticipate that many of these are already present in the vitreous oxide, given the extensive controversy over many years regarding its density.

We have explored in detail the underlying atomic mechanisms that govern this behaviour and found that the bending potentials of the flexible B-O-B bridges, when considered in isolation, are unable to account for the particularly exceptional flexibility of the boroxyl-decorated frameworks. The flexibility depends on topological and geometric factors, such as the number density of B-O-B bridges. Crucially, the incorporation of boroxyl rings into the frameworks relaxes the *torsional constraints* on the B-O-B bridges; this allows the frameworks to exploit an intrinsic cooperativity between bending and twisting motions in the bridges during expansion. The flexibility of the boroxyl-based frameworks can be significantly preserved by decoration with alternative isoelectronic rings, including triazine, borazine and benzene.

We also propose a novel approach to the prediction of further B_2O_3 polymorphs. Given any arrangement of SiO_4 tetrahedra, it is possible to construct a related structure in which the SiO_4^{4-} tetrahedra are exchanged for $B_2O_5^{4-}$ units. Calculations on a borate analogue of β-cristobalite (β-cristobalite-borate-a), constructed in such manner, shows it to be isoenergetic with the known B_2O_3-I polymorph. An enormous number of boron-oxygen polymorphs can be obtained in this way and we further predict a family of zeolite analogues. We have some evidence to suggest subtle differences are likely in the energy landscapes of the zeolites and their boron analogues; whilst the minimum energy structures of zeolites tend to lie towards the high volume end of their flexibility windows, it is expected that the borate analogues will be highly compressed in their relaxed states. To the best of our knowledge, templated synthesis of boron oxides similar to that of zeolites has not so far been attempted.

The frameworks we have examined have access to significantly larger variations in volume than well-known flexible MOFS such as MIL-53Cr. The facile collapse and expansion of the cavities that pervade the frameworks– in contrast to the vast majority of covalent organic frameworks (COFs), which form a rigid network of fixed nanochannels – opens up the prospect of novel storage capabilities and host-guest chemistry.[49,50,51,52] We hope that our work and predicted low-energy structures will further new experimental work on these fascinating systems.

Acknowledgements

HJAD acknowledges the award of a Royal Society of Chemistry Undergraduate Research Bursary. We thank Stephen Wells and Asel Sartbaeva for many discussions and their help with the GASP program.

References

[1] Themed issue: Metal Organic frameworks, *Chem. Soc. Rev.* 2009, **38**, 1201-1508
[2] A.U. Czaja, N. Trukhan and U. Müller, *Chem. Soc. Rev.* 2009, **38**, 1284
[3] P. Horcajada, R. Gref, T. Baati, P.K. Allan, G. Maurin, P. Couvreur, G. Férey, R.E. Morris and C. Serre, *Chem. Rev.*, 2012, **112**, 1232 and references therein.
[4] J.-R. Li, J. Sculley and H.-C. Zhou, *Chem. Rev.*, 2012, 112, 869
[5] H. Furukawa, K. E. Cordova, M. O'Keeffe and O. M. Yaghi, *Science*, 2013, 341, 974.
[6] A. Schneemann, S. Henke, I. Schwedler and R. A. Fischer, *ChemPhysChem*, 2014, 15, 823.
[7] G. Férey and C. Serre, *Chem. Soc. Rev.* 2009, **38**, 1380.
[8] G. Férey, *Dalton Trans.* 2016, **45**, 4073.
[9] A. Schneemann, V. Bon, I. Schwedler, I. Senkovska, S. Kaskel and R. A. Fischer, *Chem. Soc. Rev.*, 2014, 43, 6062

[10] F. X. Coudert, *Chem. Mater.* 2015, 27, 1905.
[11] E. Cockayne, *J. Phys. Chem. C*, 2017, 121, 4312.
[12] C. Mellot-Draznieks, C. Serre, S. Surblé, N. Audebrand, and G. Férey, *J. Am. Chem. Soc.*, 2005, 127, 16273.
[13] C. Serre, C. Mellot-Draznieks, S. Surblé, N. Audebrand, Y. Flinchuk and G. Férey, *Science*, 2007, 315, 1828.
[14] L. Villaescusa, P. Lightfoot, S.J. Teat and R.E. Morris, *J. Am. Chem. Soc.*, 2001, **123**, 5453.
[15] G.D. Barrera, J.A.O. Bruno, T.H.K. Barron, and N.L. Allan, J. Phys.: Condens. Matter, 2005, **17**, R217
[16] M. Jeffroy, A.H. Fuchs and A. Boutin, *Chem. Commun*. 2008, 3275
[17] G. Ferlat, A. P. Seitsonen, M. Lazzeri and F. Mauri, *Nature Mater.*, 2012, **11**, 925
[18] G. E. Gurr, P.W. Montgomery, C. D. Knutson and B. T. Gorres, *Acta. Cryst*., 1970, **26**, 906
[19] C. T. Prewitt and R. D. Shannon, *Acta. Cryst*., 1968, **24**, 869
[20] G. Ferlat, T. Charpentier, A. P. Seitsonen, A. Takada, M. Lazzeri, L. Cormier, G. Calas and F. Mauri, *Phys. Rev. Lett*., 2008, **101**, 65504
[21] P. Umari, and A. Pasquarello, *Phys. Rev. Lett*., 2005, **95**, 13401
[22] L. Huang, M. Durandurdu and J. Kieffer, *J. Phys. Chem*., 2007, **111**, 13712
[23]A. Takada, C. R. A. Catlow and G. D. Price, *Phys. Chem. Glasses*, 2003, **44**, 147
[24] F. Claeyssens, J. N. Hart, N. C. Norman and N. L. Allan, *Adv. Funct. Mater*., 2013, **23**, 5887
[25] J. Carrasco, F. Illas and S.T. Bromley, *Phys. Rev. Lett.* 2007, **99**, 235502.
[26] M.A. Zwijnenburg and S.T. Bromley, *Phys. Rev. B* 2011, **83**, 024104.
[27] M.A. Zwijnenburg and S.T. Bromley, *J. Mat. Chem.* 2011, **21**, 15255.
[28] W. Sangthong, J. Limtrakul, F. Illas and S.T. Bromley, *J. Mat. Chem.* 2008**, 18**, 5871.
[29] M.-S. Wang, G.-C. Guo, W.-T. Chen, G. Xu, W.-W. Zhou, K.-J. Wu and J.-S. Huang *Angew. Chem. Int. Ed.* 2007, **46**, 3909.
[30] M.-C. Liu, P. Zhou, H.-G. Yao, S.-H. Ji, R.-C. Zhang, M. Ji and Y.-L. An *Eur. J. Inorg. Chem.* 2009, **31**, 4622.
[31] F. Claeyssens, N.L. Allan, N.C. Norman, and C.A. Russell, *Phys. Rev. B* 2010, **82**, 094119
[32] R. J. Bell and A. Carnevale, *Phil. Mag*., 1982, **43**, 389
[33] S. J. Clark, M. D. Segall, C. J. Pickard, P. J. Hasnip, M. J. Probert, K. Refson, M. C. Payne, *Z. Kristallogr*., 2005, **220**, 567
[34] J. P. Perdew, K. Burke and M. Ernzerhof, *Phys. Rev. Lett*., 1996, **77**, 3865
[35] J. P. Perdew and Y. Wang, *Phys. Rev. B*, 1992, **45**, 13244
[36] D. Vanderbilt, *Phys. Rev. B*, 1990, **41**, 7892
[37] H. J. Monkhorst and J. D. Pack, *Phys. Rev. B*, 1976, **13**, 5188
[38] Gaussian 09, Revision D.01, M. J. Frisch, G. W. Trucks, H. B. Schlegel, G. E. Scuseria, M. A. Robb, J. R. Cheeseman, G. Scalmani, V. Barone, G. A. Petersson, H. Nakatsuji, X. Li, M. Caricato, A. Marenich, J. Bloino, B. G. Janesko, R. Gomperts, B. Mennucci, H. P. Hratchian, J. V. Ortiz, A. F. Izmaylov, J. L. Sonnenberg, D. Williams-Young, F. Ding, F. Lipparini, F. Egidi, J. Goings, B. Peng, A. Petrone, T. Henderson, D. Ranasinghe, V. G. Zakrzewski, J. Gao, N. Rega, G. Zheng, W. Liang, M. Hada, M. Ehara, K. Toyota, R. Fukuda, J. Hasegawa, M. Ishida, T. Nakajima, Y. Honda, O. Kitao, H. Nakai, T. Vreven, K. Throssell, J. A. Montgomery, Jr., J. E. Peralta, F. Ogliaro, M. Bearpark, J. J. Heyd, E. Brothers, K. N. Kudin, V. N. Staroverov, T. Keith, R. Kobayashi, J. Normand, K. Raghavachari, A. Rendell, J. C. Burant, S. S. Iyengar, J. Tomasi, M. Cossi, J. M. Millam, M. Klene, C. Adamo, R. Cammi, J. W. Ochterski, R. L. Martin, K. Morokuma, O. Farkas, J. B. Foresman, and D. J. Fox, Gaussian, Inc., Wallingford CT, 2016.
[39] NBO Version 3.1, E. D. Glendening, A. E. Reed, J. E. Carpenter, and F. Weinhold.
[40] S. A. Wells and A. Sartbaeva, *Mol. Simulat.*, 2015, **41**, 1409.
[41] F. Gatti, N. Berthe-Gujac, I. Demachy and F. Voltatron, *Chem. Phys. Lett*., 1995, **232**, 503
[42] R. M. Minyaev and E. A. Lepin, *Mendeleev Commun.*, 1997, **7**, 80
[43] F. Wiitkar, S. Kahlal, J. F. Halet, J. Y. Saillard, J. Bauer and P. J. Rogl, *Am. Chem. Soc.*, 1994, **116**, 251
[44] S. A. Wells, K.M. Lueng, P.P. Edwards, M.G. Tucker and A. Sartbaeva, *Roy. Soc. Open Sci.*, 2017, **4**, 170757.
[45] A. Sartbaeva, S. A. Wells, M. M. J. Treacy and M. F. Thorpe, *Nat. Mater. Lett*., 2006, **5**, 962
[46] D. S. Wragg, R. E. Morris and A. W. Burton, *Chem. Mater.*, 2008, **20**, 1561
[47] W. H. Baur, *Acta. Cryst*., 1980, **36**, 2198
[48] L. Huang and J. Kieffer, *Phys. Rev.*, 2006, **74**, 224107
[49] A. P. Côté, A. I. Benin, N. W. Ockwig, M. O'Keeffe, A. J. Matzger, O. M. Yaghi, *Science*, 2005, **310**, 1166
[50] S. Y. Wang and W. Wang, *Chem. Soc. Rev*., 2013, **42**, 548
[51] P. J. Waller, F. Gandara and O. M. Yaghi, *Acc. Chem. Res*., 2015, **48**, 3053
[52] H. Xu, J. Gao and D. Jiang, *Nat. Chem.*, 2015, **7**, 905